



Tuning enantioselectivity in asymmetric hydrogenation of acetophenone and its derivatives via confinement effect over free-standing mesoporous palladium network catalysts



Yu Wang^{a,b}, Na Su^a, Lin Ye^a, Yuanhang Ren^a, Xueying Chen^{a,*}, Yujue Du^c, Zhenhua Li^a, Bin Yue^a, Shik Chi Edman Tsang^d, Qiao Chen^e, Heyong He^{a,*}

^a Department of Chemistry and Shanghai Key Laboratory of Molecular Catalysis and Innovative Materials, Collaborative Innovation Center of Chemistry for Energy Materials, Fudan University, Shanghai 200433, PR China

^b School of Chemical and Environmental Engineering, Shanghai Institute of Technology, Shanghai 201418, PR China

^c Shanghai Research Institute of Petrochemical Technology, SINOPEC, Shanghai 201208, PR China

^d Wolfson Catalysis Centre, Department of Chemistry, University of Oxford, Oxford OX1 3QR, UK

^e Department of Chemistry, School of Life Sciences, University of Sussex, Brighton BN1 9QJ, UK

ARTICLE INFO

Article history:

Received 10 January 2014

Revised 5 March 2014

Accepted 8 March 2014

Keywords:

Confinement effect
Enantioselective hydrogenation
Mesoporous palladium
Acetophenone
Aromatic ketone
Proline
Molecular modeling

ABSTRACT

The confinement effect on enantioselective hydrogenation of acetophenone and its derivatives over free-standing mesoporous Pd network catalysts was systematically studied. It was found for the first time that the enantiomeric excess (ee) could be effectively tuned by altering the confinement effect optimized by precise control of the topology, pore size, and lattice structure of mesoporous Pd catalysts. The double gyroid structure with proper pore size and desired lattice structure formed by KBH_4 reduction provided suitable microenvironment to generate optimized confinement effect. The optimized catalyst exhibited ee of 40–73% at 273 K under atmospheric pressure of H_2 . DFT study revealed that the major enantiomeric product could be predicted by comparing relative energies of prochiral-R and -S complexes formed by acetophenone derivatives with S-proline. The energetically favored complex led to the formation of the corresponding enantiomer in excess upon hydrogenation, and ee was found to be linearly correlated with the energy difference between prochiral-R and -S complexes.

© 2014 Elsevier Inc. All rights reserved.

1. Introduction

The steady growing of high demand for efficacious and safe chiral drugs has provided great inspiration to develop effective asymmetric synthesis methods for preparing single-enantiomer chemicals [1]. Heterogeneous enantioselective hydrogenation is one of the most ideal methods for the synthesis of enantio-pure compounds. It provides a versatile access to diverse types of important chiral drug intermediates in pharmaceutical industries such as chiral amines and alcohols by simply hydrogenating the corresponding unsaturated prochiral imines and ketones [2]. Moreover, heterogeneous enantioselective hydrogenation process is intrinsically atom-economical as compared to other reduction methods [3]. In addition, heterogeneous catalysts possess many technical processing advantages such as ease of handling, separation, and recycling of solid catalysts in comparison with

the homogeneous counterparts [4], which have obvious advantages in green chemistry. Thus, heterogeneous enantioselective hydrogenation is in the forefront of both academic and industrial researches over recent years [2,5].

The success of developing effective heterogeneous enantioselective catalysts relies on the structural optimization for a fine balance of reactivity and chiral selectivity in terms of conversion and enantiomeric excess (ee). Here, we choose the enantioselective hydrogenation of aromatic ketones (such as acetophenone) as a model system for quantitatively evaluating the catalytic properties of our newly developed free-standing mesoporous Pd network catalysts in contrast to the conventional supported metal catalysts [6–18]. Tugler et al. studied the enantioselective hydrogenation of acetophenone over S-proline modified Pd/C, and the ee of 22% was achieved at 78% conversion [6]. Perosa et al. studied the enantioselective hydrogenation of acetophenone over cinchona-modified Pt/C which gave 20% ee [7]. Baiker et al. studied the enantioselective hydrogenation of acetophenone or ring-substituted acetophenones over cinchonidine-modified Pt/ Al_2O_3 [8,9] and Rh/ Al_2O_3 catalysts [10]. They found that the introduction of

* Corresponding authors. Fax: +86 21 5566 5572.

E-mail addresses: xueyingchen@fudan.edu.cn (X. Chen), heyonghe@fudan.edu.cn (H. He).

electron-withdrawing functional groups in the aromatic ring increased the enantioselectivity with up to 69% ee obtained in the hydrogenation of 3,5-di(trifluoromethyl)acetophenone. Vetere et al. investigated the enantioselective hydrogenation of acetophenone over chiral organotin-modified Pt/SiO₂ catalysts which produced ca. 20% ee [11]. Basu et al. studied the asymmetric hydrogenation of acetophenone over MCM-41 supported [Pt₁₂(CO)₂₄]²⁻-derived catalysts, and 49% ee was achieved with the acetophenone conversion of 40% [12]. Marzioletti et al. studied the enantioselective hydrogenation of acetophenone on cinchonidine-modified Ir/SiO₂ catalyst, and up to 62% ee was claimed despite the fact that it required a very high cinchonidine concentration [13]. Recently, it was reported that immobilized Ru and Ir metal complexes with chiral diamine ligands exhibited good enantioselectivity (60–96% ee) in the enantioselective hydrogenation of aromatic ketones, but the leaching of Ru and Ir to the organic solvent may be a problem [14–20].

It is known that the weak interaction between reactant and catalyst support (such as van der Waals forces, hydrogen bonding, and physical adsorption) is in the same order of magnitude as the energy difference between the two transition states of R- and S-products in chiral reactions [21]. Thus, the additional interactions with the support can significantly affect the enantioselectivity. Recently, Baiker and coworkers reported that by tuning the acid-base properties of the Al₂O₃ support, the enantioselectivity of hydrogenation reaction can be altered [22,23]. Therefore, the presence of support adds the complexity in the study of heterogeneous enantioselective hydrogenation reactions in elucidating the origin of the enantioselectivity and the nature of the chiral recognition on metal catalysts.

Recently, free-standing mesoporous metals with highly ordered and interconnected networks have shown great potentials in heterogeneous catalysis owing to their synergetic advantages of native catalytic activity of the metal along with the large surface area, well-defined mesostructures and controllable pore size distributions [24–31]. For asymmetric hydrogenation reactions, free-standing mesoporous metals have the following advantages. Firstly, the effect of support is completely eliminated, which significantly reduces the complexity and difficulty in the study of the mechanism of heterogeneous enantioselective hydrogenation reactions. Secondly, the confinement effect within the mesoporous metals can be precisely managed by controlling the pore shape, pore size, and pore wall thickness of the original silica templates. This provides us good opportunities to study the details of the confinement effect, allowing fine tuning of the enantioselectivity [21].

Previously, we reported that an S-proline-modified Pd nanoarray catalyst with hexagonal mesostructure exhibited superior ee over Pd black in the enantioselective hydrogenation of acetophenone due to the confinement effect [32]. However, the structural factors influencing the confinement effect and their correlations with the enantioselectivity remain to be clarified. The precise control of the nanoporosity and the lattice properties of the mesoporous Pd catalyst may allow us to optimize the confinement effect and further improve the enantioselectivity in the hydrogenation process. Thus, the aim of the present work is to systematically investigate the confinement effect over the free-standing mesoporous Pd catalysts and to gain insights into enantioselective hydrogenation over such metal surfaces. We synthesized a series of free-standing mesoporous Pd network catalysts with different topologies (space group of I4₁32, Ia3d, and P6mm), pore sizes, and lattice structures by the hard templating method. With the enantioselective hydrogenation of acetophenone as a probe, the relationship between the enantioselectivity and structure can be obtained. Hydrogenation of ring-substituted acetophenones was also performed for evaluating how the enantioselectivities were affected by the interactions of prochiral compounds with the mesoporous

Pd surfaces. For a better understanding of the chiral recognition on the Pd surface, the bonding and interaction of the chiral modifier with acetophenone and its derivatives on a Pd surface were also investigated using density functional theory (DFT) calculations. The structures of the enantio-differentiating intermediate complexes were identified and their adsorption energies were obtained.

2. Experimental

2.1. Catalyst preparation

A series of mesoporous Pd network catalysts with 3D gyroid structure and different pore sizes were prepared as follows. KIT-6 mesoporous silica templates were synthesized at different hydrothermal treatment temperatures of 308, 353, 373, and 403 K according to the literature [33]. 1.00 g of KIT-6 was added into 40 mL of hexane and stirred vigorously for 30 min. An aqueous solution of H₂PdCl₄ (0.56 M) was then added dropwise under vigorous stirring and ultrasonication. The volume ratio of the H₂PdCl₄ solution to the pore of the silica template was ca. 1.5. The excessive solution was decanted and the resulting solids were dried overnight at 393 K. The impregnation was repeated several times in order to achieve high Pd loadings of ca. 25–55 wt.% with respect to the silica template. The resulting powders were reduced by aqueous solution of KBH₄ (0.3 M) or N₂H₄·H₂O at ambient conditions or by H₂ at 573 K for 2 h. The black solids obtained were treated by hydrofluoric acid to dissolve the silica template. The products were washed with distilled water until neutrality and then with methanol three times. The catalysts were kept in methanol for characterization and activity test.

The parent KIT-6 templates, the Pd-loaded KIT-6 samples, and the silica-free mesoporous Pd network catalysts were designated as KIT-*x*, Pd-*y*/KIT-*x*, and Pd-*x*-*y*, respectively, where *x* refers to the hydrothermal treatment temperature of original KIT-6 template and *y* refers to the reducing agent. For comparison, ultrafine Pd black and hexagonal Pd nanoarray [32] were also prepared by similar procedure using KBH₄ as the reducing agent. It should be noted that the as-prepared mesoporous Pd network catalysts are pyrophoric; thus, care must be taken to preclude them from air exposure during sample handling and disposal.

2.2. Characterization

The chemical compositions of the catalysts were analyzed by inductively coupled plasma-atomic emission spectroscopy (ICP-AES, Thermo Elemental IRIS Intrepid). The FTIR spectra were recorded on a NEXUS 470 FTIR spectrometer. The BET specific surface area and pore volume were measured by N₂ adsorption at 77 K on a Quantachrome Quadrasorb SI apparatus. Prior to the measurement, the catalyst was transferred to a glass tube and degassed at 383 K under N₂ flow for 2 h. The pore volume was calculated from the amount of N₂ adsorbed at a relative pressure of 0.995. The pore size distribution was calculated from the desorption branch of the isotherms using the Barrett-Joyner-Halenda (BJH) algorithm.

The active surface area was measured by pulsed CO chemisorption on a Micromeritics ChemiSorb 2750, assuming CO/Pd(s) = 0.6 and a surface area of 7.874 × 10⁻²⁰ m² per Pd atom [34]. The turnover frequency (TOF) was expressed as the number of acetophenone and its derivatives consumed per active surface Pd atom per second.

The low-angle and wide-angle X-ray diffraction (XRD) patterns were recorded on a Bruker D4 Endeavor X-ray diffractometer and a Bruker AXS D8 Advance X-ray diffractometer, respectively, using Cu Kα radiation. The catalyst with methanol was loaded in an in

situ cell purged with Ar (99.9995%) during the analysis to avoid air oxidation. The mean crystallite size of Pd was obtained from the peak width of the Pd(111) reflection using the Scherrer equation [35].

The mesostructure, selected-area electron diffraction (SAED) pattern, and elemental analysis of the catalysts were acquired on a JEOL 2011 transmission electron microscope (TEM) operated at 200 kV and fitted with an energy dispersive X-ray emission analyzer (EDX). High-resolution scanning electron microscopy (HRSEM) images were taken on a Hitachi S-4800 ultrahigh-resolution scanning electron microscope operated at 20 kV equipped with a cold field emission gun (FEG) and an in-lens electron optics. The structure modeling of the mesoporous Pd replicas with the single or double gyroid structure was carried out using the density distribution function developed for gyroid mesostructure according to the literature [36].

Density functional theory (DFT) calculation of the adsorption geometries and energies was performed using the SIESTA package with numerical atomic orbital basis sets and Troullier–Martins norm-conserving pseudopotentials [37,38]. The exchange–correlation functional utilized is the generalized gradient approximation PBE method, known as GGA-PBE [39]. A double-polarization basis set (DZP) was employed. The orbital-confining cutoff radii were determined from an energy shift of 0.01 eV. The energy cutoff for the real space grid used to represent the density was set as 150 Rydberg. To further speed up calculations, the Kohn–Sham equations were solved by an iterative parallel diagonalization method that utilized the ScaLAPACK subroutine pdsygvx with two-dimensional block cyclically distributed matrix [40]. The Broyden method was employed for geometry relaxation until the Cartesian forces on each relaxed atom were all less than 0.05 eV Å⁻¹. A four-atomic-layer periodic slab with top half of atoms allowed to relax was used to simulate the Pd(111) surface. A (5 × 5) surface unit cell was used to study the adsorptive conformations of S-proline with acetophenone. The slabs were separated from their periodic images in the direction perpendicular to the surface by interposing an adequate amount of empty space (more than 15 Å). The Monkhorst–Pack *k*-point sampling of (3 × 3 × 1) was utilized. The optimized lattice constant was 3.95 Å for bulk Pd, which was consistent with the experimental result [41]. Spin polarization was considered during all the calculations. Adsorption energies were calculated as follows:

$$E_{\text{ads}} = E_{\text{proline-acetophenone complex+Pd(111)}} - E_{\text{Pd(111)}} - E_{\text{proline}} - E_{\text{acetophenone}}$$

where $E_{\text{proline-acetophenone complex+Pd(111)}}$ is the total energy of the coadsorbed S-proline and acetophenone on the Pd(111) surface, $E_{\text{Pd(111)}}$ is the energy of the isolated Pd(111) surface, E_{proline} and $E_{\text{acetophenone}}$ are the energy of the S-proline and acetophenone molecules in vacuum, respectively.

2.3. Activity test and product analysis

The activity test was carried out in a 100 mL glass flask with a magnetic stirrer in H₂ at atmospheric pressure with a flow rate

of 60 mL min⁻¹. Methanol was used as the solvent. The reaction conditions were as follows: 0.02 mL of acetophenone, 0.40 g of S-proline, 17 mL of methanol, 0.050 g of Pd catalyst, stirring rate of 1000 rpm to exclude diffusion effects, and reaction temperature of 273 K. The products were identified by GC/MS. Conversion and enantioselectivity were determined by a GC equipped with an Agilent HP-CHIRAL (19091G-B213) capillary column and a FID detector. The enantioselectivity is expressed as ee (%) = 100 × |(R – S)| / (R + S). The assignment of the absolute configuration of the product was based on the retention times in GC analysis. Reproducibility of ee was within ±0.5%.

3. Results and discussion

3.1. Catalyst texture

The BET specific surface area, pore volume, pore diameter and wall thickness of the parent KIT-6 templates prepared at different hydrothermal treatment temperatures, are presented in Table 1. The BET specific surface areas of all the KIT-6 are higher than 400 m² g⁻¹. The pore volumes of the KIT-6 samples strongly depend on the hydrothermal treatment temperature. Higher hydrothermal treatment temperature results in larger pore volume. It is worth noting that for successful preparation of the mesoporous Pd network catalyst, the exact pore volume of the parent KIT-6 templates has to be known, so the minimum volume of H₂PdCl₄ solution added can be adjusted accordingly. The wall thickness was calculated according to the literature [42] based on the BJH pore size obtained from the desorption branch of the isotherm and the unit cell parameter obtained from XRD data. The wall thickness of KIT-6 samples is also influenced by the hydrothermal treatment temperature, decreasing from 5.8 nm at 308 K to 2.6 nm at 403 K. The KIT-6 prepared at 308 K features the smallest mesopore diameter with the thickest wall, which is in line with the reported results [33].

The nitrogen adsorption–desorption isotherms and the corresponding pore size distribution curves of the KIT-6 samples are shown in Fig. 1a and b, respectively. The isotherms of all the KIT-6 samples (Fig. 1a) exhibit a type IV shape with a hysteresis above P/P_0 of 0.4, revealing the presence of mesopores. The relative pressure at the appearance of the hysteresis loop increases with increasing the hydrothermal treatment temperature, indicating the increase in the pore dimensions. The narrow pore size distribution curves (Fig. 1b) indicate the uniform mesopores of the KIT-6 samples. The pore diameter of the KIT-6 samples increased from 4.0 to 9.8 nm when the hydrothermal treatment temperature was increased from 308 to 403 K.

Fig. 2 displays the N₂ adsorption–desorption isotherms and pore size distribution curves of the replicated silica-free Pd catalysts. Their BET specific surface areas, pore volumes and pore diameters are summarized in Table 2. Generally, the BET specific surface areas ranging from 45 to 80 m² g⁻¹ were observed over the silica-free Pd samples, which are significantly larger than the ultrafine Pd black sample (23 m² g⁻¹). ICP-AES analysis revealed that no boron or potassium was detectable in the silica-free KBH₄-reduced Pd catalysts, excluding the contamination of Pd with potassium or

Table 1
Physicochemical properties of parent KIT-6 samples.

Sample	S_{BET} (m ² g ⁻¹)	V_{pore} (cm ³ g ⁻¹)	$d_{\text{pore}}^{\text{a}}$ (nm)	Unit cell parameter (nm)	Wall thickness ^b (nm)
KIT-308	523	0.49	4.0	19.6	5.8
KIT-353	507	0.68	4.9	20.2	5.2
KIT-373	707	1.13	6.8	23.3	4.9
KIT-403	435	1.60	9.8	24.7	2.6

^a Calculated from the desorption branch of the isotherm using the BJH model.

^b Calculated according to Ref. [42].

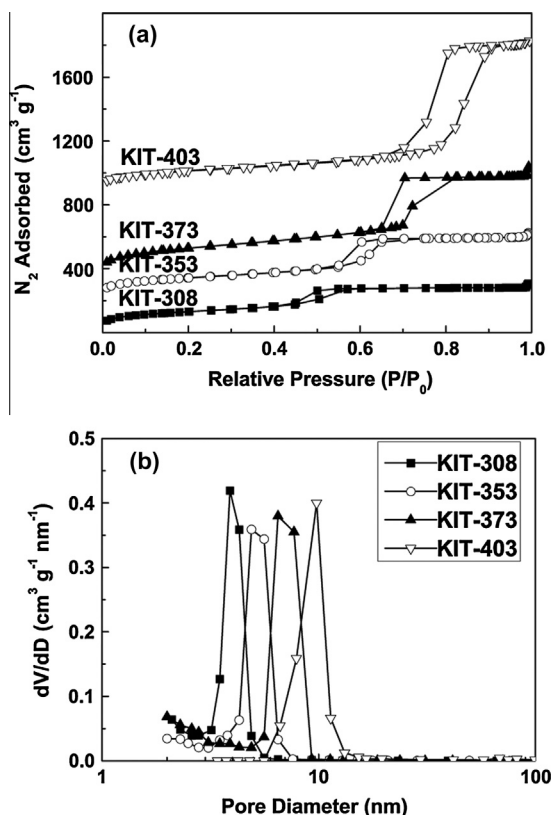


Fig. 1. N_2 adsorption–desorption isotherms (a) and pore size distribution curves (b) of parent KIT-6 samples synthesized at different hydrothermal treatment temperatures.

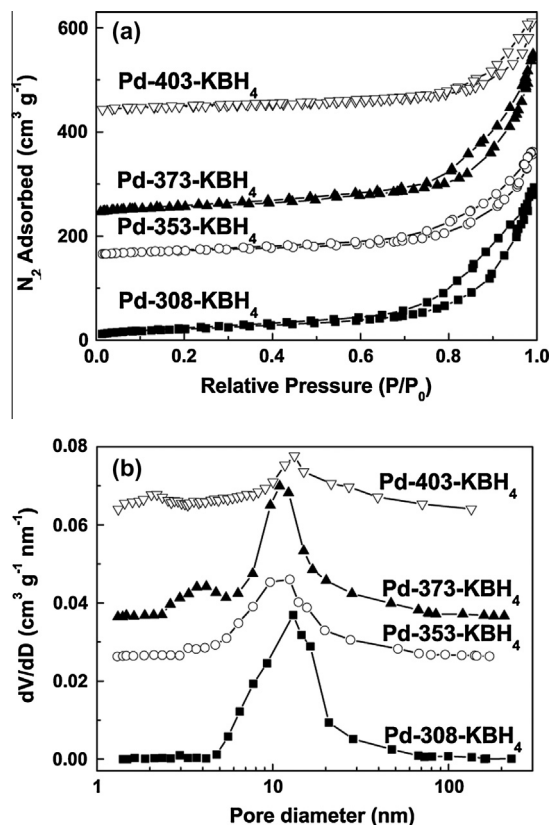


Fig. 2. N_2 adsorption–desorption isotherms (a) and pore size distribution curves (b) of silica-free mesoporous Pd catalysts prepared using parent KIT-6 synthesized at different hydrothermal treatment temperatures.

boron. As shown in Fig. 2a, the silica-free Pd samples also exhibited a type IV isotherm with H_3 hysteresis loops, indicative of their mesoporous structure. For the Pd-308-KBH₄ and Pd-353-KBH₄ samples, only single narrow pore size distribution was observed (Fig. 2b). The pore sizes are ca. 11–13 nm, which are much larger than the wall thickness of the silica template (5.8–2.6 nm). The presence of these large mesopores may relate to the special structure of the KIT-6 template [42,43]. It is well known that the 3D bicontinuous gyroidal KIT-6 with space group of Ia3d consists of two sets of interpenetrating mesopores and the pore interconnectivity is influenced by the hydrothermal treatment temperature. The low hydrothermal treatment temperature usually results in a decreased interconnectivity [33]. Thus, during Pd replication from KIT-6 prepared at low temperatures (KIT-308 and KIT-353), the reduction and accretion of Pd occur in the two sets of mesopores separately in KIT-6, forming uncoupled gyroid Pd networks with the pore diameters of 13.1 and 11.0 nm, which are close to the dimensions of two silica walls (5.8 and 5.2 nm) [42]. For the Pd-373-KBH₄ and Pd-403-KBH₄ samples, although the large mesopore at ca. 11–13 nm could be still observed, a new peak at 4.1 nm (Pd-373-KBH₄) or 2.1 nm (Pd-403-KBH₄) arose. Such a bimodal pore size distribution is similar to the case of mesoporous NiO and MoO₂ replicas [44,45]. The diameter of the mesopores at ca. 4.1 and 2.1 nm is close to the wall thickness of the parent KIT-373 and KIT-403 templates. This represents a good quality of replication, which is related to the higher interconnectivity in KIT-6 prepared at high temperatures, allowing better mass transportation [42,44].

3.2. Topology

Fig. 3 shows the low-angle XRD patterns of the parent KIT-6 templates. All the KIT-6 samples exhibit typical diffraction peaks that are characteristic of 3D gyroidal mesostructures [45]. The unit cell parameters of the KIT-6 samples calculated based on the $d_{(211)}$ -spacing value from the XRD patterns are listed in Table 1. The unit cell parameters are in the range of 19.6–24.7 nm and increase with increasing the hydrothermal treatment temperature.

The low-angle XRD patterns of the silica-free Pd catalysts strongly depend on the hydrothermal treatment temperature of the parent silica templates. For KIT-6 synthesized at high temperatures (≥ 373 K), similar diffraction patterns of the resulted Pd network catalysts (Pd-373-KBH₄ and Pd-403-KBH₄) were achieved. Fig. 4a shows the low-angle XRD patterns of samples at different stages of impregnation using KIT-373 as a template. After the incorporation of Pd in the parent KIT-373 template, the intensity of all the diffraction peaks in Pd-KBH₄/KIT-373 decreased dramatically and only the strongest (211) reflection for Ia3d symmetry [42] was clearly observed at $2\theta \approx 1.00^\circ$. However, by removing the Pd networks from Pd-KBH₄/KIT-373 using aqua regia, the diffraction peaks of the KIT-373 silica template were fully recovered despite a slight shift of all the diffraction peaks to larger angles. Thus, the diffraction intensity difference between KIT-373 and Pd-KBH₄/KIT-373 is not due to the lowering of structural regularity of the parent silica template. On the other hand, no significant change of the diffraction peak was observed before (Pd-KBH₄/KIT-373) and after removal of KIT-6 template (Pd-373-KBH₄). Therefore, we can conclude that once loaded with Pd, the overall diffraction peaks were dominated by the reflection from the Pd structures, overshadowing the silica. The reduction in the diffraction peak intensity in the Pd-loaded samples may be attributed to the different X-ray absorption characteristics of Pd compared to silica [46]. Compared to the parent KIT-6, the (211) reflection of the Pd-373-KBH₄ sample shifted slightly to larger angles, indicating a small shrinkage of the Pd mesostructure after replication.

Table 2
Physicochemical properties of silica-free mesoporous Pd catalysts.

Catalyst	S_{BET} ($\text{m}^2 \text{g}^{-1}$)	V_{pore} ($\text{cm}^3 \text{g}^{-1}$)	$d_{\text{pore}}^{\text{a}}$ (nm)	Wall thickness ^b (nm)
Pd-308-KBH ₄	78	0.47	13.1	4.3
Pd-353-KBH ₄	65	0.38	11.0	5.3
Pd-373-KBH ₄	78	0.49	4.1, 11.0	7.4
Pd-403-KBH ₄	46	0.27	2.1, 13.3	9.7
Pd-373-N ₂ H ₄ ·H ₂ O	51	0.31	12.2	7.4
Pd-373-H ₂	39	0.38	14.5	7.4
Ultrafine Pd black	23	0.19	42.5	–

^a Calculated from the desorption branch of the isotherm using the BJH model.

^b Determined from TEM analysis.

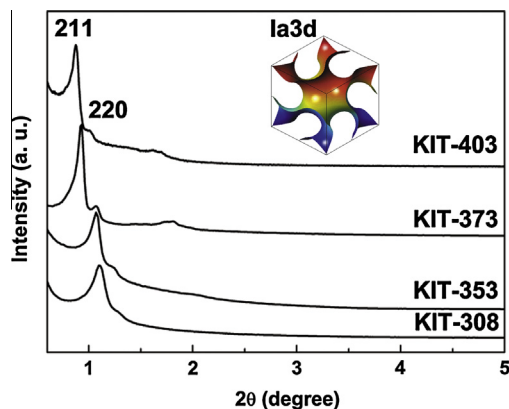


Fig. 3. Low-angle XRD patterns and structure model (inset) of the parent KIT-6 samples synthesized at different hydrothermal treatment temperatures.

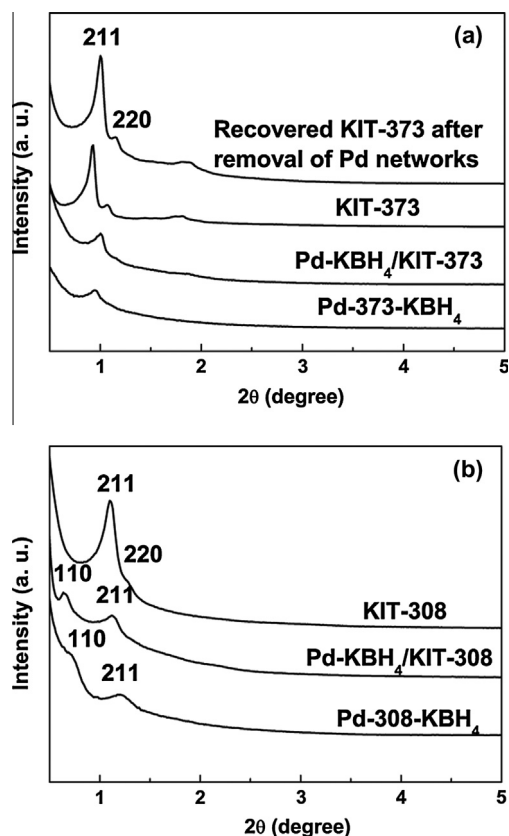


Fig. 4. Low-angle XRD patterns of (a) KIT-373, Pd-KBH₄/KIT-373, silica-free Pd-373-KBH₄ and recovered KIT-373 after the removal of the Pd networks; (b) KIT-308, Pd-KBH₄/KIT-308 and silica-free Pd-308-KBH₄ samples.

Based on these XRD results, the aforementioned N₂ physisorption data and the following TEM and HRSEM observations (dominance of double gyroid networks), it is therefore reasonable to infer that due to the large pore size and higher interconnectivity of the KIT-6 samples prepared at high temperatures (KIT-373 and KIT-403), the resulted mesoporous Pd networks replicated the structure of the parent silica very well and the Ia3d symmetry was preserved [47].

When KIT-6 samples prepared at low temperatures (≤ 353 K) were used as the templates, the diffraction patterns of the resulted Pd-308-KBH₄ and Pd-353-KBH₄ are similar, but quite different from those for Pd-373-KBH₄ and Pd-403-KBH₄, as shown in Fig. 4b. Besides the (211) reflection at $2\theta \approx 1.10^\circ$, a new peak appeared at $2\theta \approx 0.64^\circ$, which was retained even after the complete removal of the silica template. This new diffraction peak can be indexed to the forbidden (110) reflection for Ia3d symmetry [48]. The appearance of the (110) peak suggested the transformation of the symmetry from cubic Ia3d to I4₁32 [42,48], which was further verified by the dominance of single uncoupled networks in the following TEM and HRSEM results.

3.3. Phase and lattice structure

The wide-angle XRD patterns of the silica-free Pd catalysts reduced by KBH₄, N₂H₄·H₂O and H₂ are shown in Fig. 5. There are four Pd diffraction peaks at 2θ of 39.3–40.1°, 45.5–46.6°, 67.0–68.1° and 79.6–82.1°, which can be indexed to (111), (200), (220) and (311) reflections of cubic fcc Pd (JCPDS No. 89-4897), respectively. The lattice constant a of the Pd-373-KBH₄, Pd-373-N₂H₄·H₂O and Pd-373-H₂ catalysts is 0.397, 0.393 and 0.389 nm, respectively. The lattice constant of the Pd network reduced by H₂ at 573 K is close to that of the bulk Pd (0.389 nm, JCPDS No. 89-4897), while reduction by KBH₄ solution gives the largest lattice distortion. The crystallite sizes of Pd in Pd-373-KBH₄, Pd-373-N₂H₄·H₂O and Pd-373-H₂

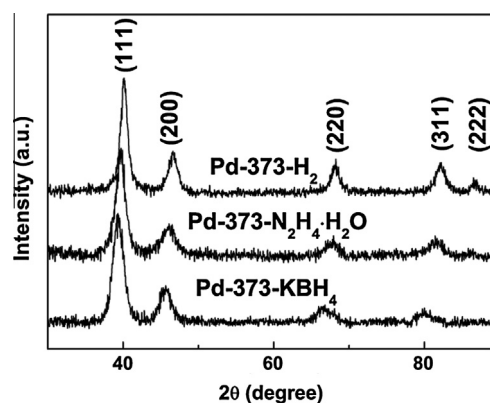


Fig. 5. Wide-angle XRD patterns of silica-free mesoporous Pd catalysts prepared using different reducing agents.

catalysts calculated using Scherrer equation are ca. 5.0, 5.5 and 8.1 nm, respectively. The relative degree of preferred orientation among crystal planes was calculated by evaluating the texture coefficient (TC) using the Harris method [49]:

$$TC_{(hkl)} = n \frac{I_{(hkl)}/I_{0(hkl)}}{\sum_{i=1}^n I_{(hkl)}/I_{0(hkl)}}$$

where $I_{(hkl)}$, $I_{0(hkl)}$ and n are the measured intensities of the mesoporous Pd catalysts studied, the standard intensities for a completely random sample obtained from JCPDS and the number of reflections, respectively. Calculation results show that the texture coefficient of the (111) plane in the Pd-373-H₂, Pd-373-N₂H₄·H₂O and Pd-373-KBH₄ catalysts is 1.00, 1.23 and 1.33, respectively. This means that there is no preferred orientation in the Pd-373-H₂ catalyst, while the Pd-373-N₂H₄·H₂O and Pd-373-KBH₄ catalysts have the preferred orientation of the (111) plane. Among the above three

catalysts, the Pd-373-KBH₄ catalyst has the highest degree of the preferred orientation of the (111) plane.

3.4. Mesoporous structure

Fig. 6 exhibits the representative TEM images of the replicated silica-free Pd catalysts. It is clear that the preparation temperature of KIT-6 can significantly affect the mesoporous structures of the resulted Pd networks. The Pd-308-KBH₄ sample (Fig. 6a and b) was composed of 3D regular networks of Pd nanowires with the diameter of ca. 4.3 nm. Only single uncoupled gyroid networks with I4₁32 symmetry (Fig. 6e) analogous to the case of CMK-1 [36,50] could be observed. This observation is supported by the appearance of the forbidden gyroid (110) diffraction peak in the low-angle XRD patterns. EDX reveals that the nanowires are composed of Pd with no detectable Si, indicating the complete removal

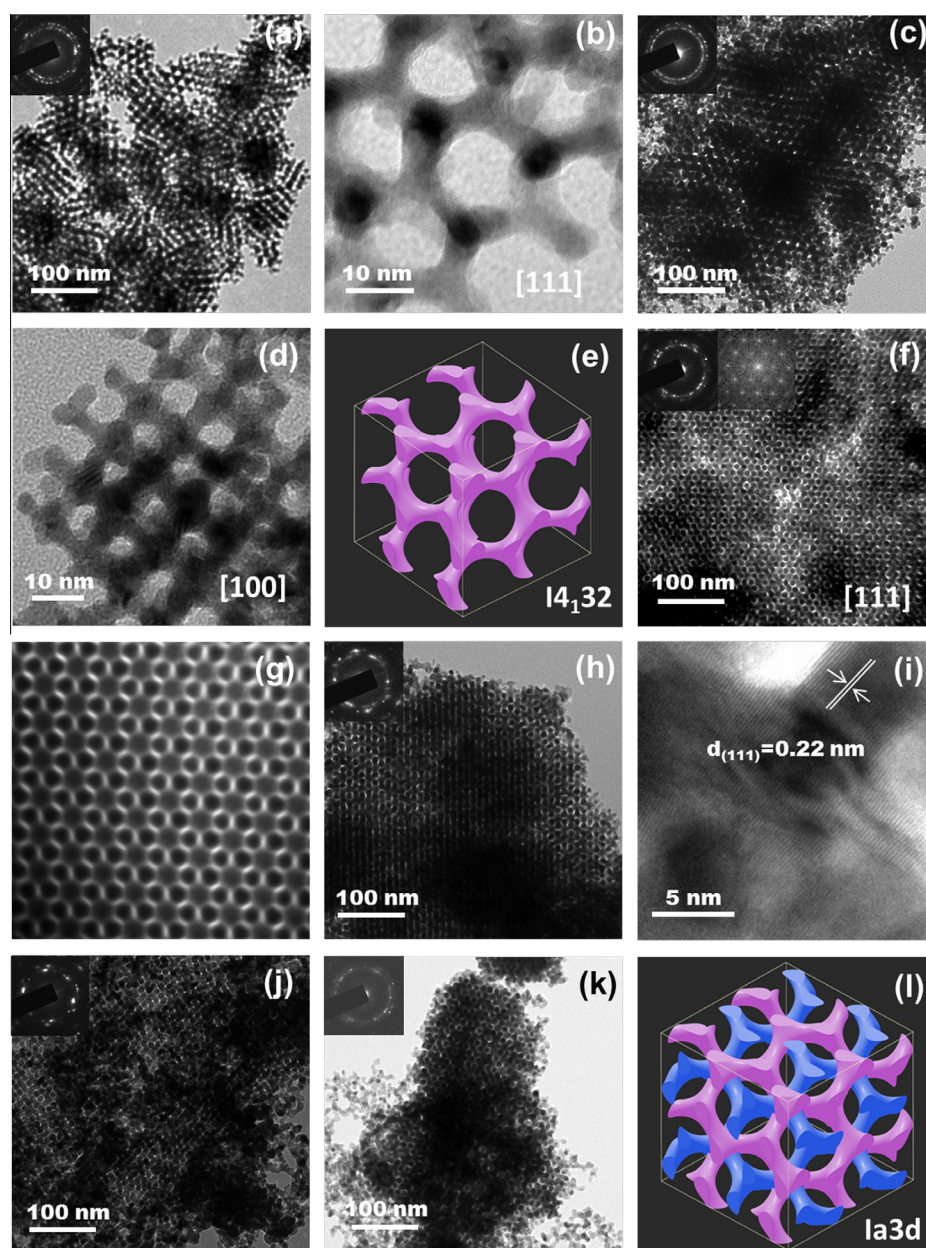


Fig. 6. TEM images of silica-free mesoporous Pd network catalysts. (a, b) Pd-308-KBH₄, (c, d) Pd-353-KBH₄, (e) skeletal model of a fragment of single gyroid with I4₁32 symmetry, (f) Pd-373-KBH₄, (g) TEM image simulation of Pd-373-KBH₄, (h, i) Pd-403-KBH₄, (j) Pd-373-H₂, (k) Pd-373-N₂H₄·H₂O and (l) skeletal model of a fragment of double gyroid with Ia3d symmetry. Insets are the corresponding SAED patterns and Fourier diffractogram.

of the silica template. The SAED pattern (the inset in Fig. 6a) displays typical polycrystalline diffraction rings assignable to fcc metallic Pd. The Pd-353-KBH₄ sample (Fig. 6c and d) exhibits a remarkable resemblance to the Pd-308-KBH₄ with slightly larger Pd nanowire diameter of ca. 5.3 nm.

KIT-6 samples prepared at high temperatures (≥ 373 K) form well-coupled double gyroid networks with even larger Pd nanowire diameters (Fig. 6f and h). The Fourier diffractogram (the insets in Fig. 6f), the TEM image simulations (Fig. 6g) and the structure modeling (Fig. 6i) clearly verify the Ia3d symmetry of such double gyroid structures [47]. The diameters of the Pd nanowires in Pd-373-KBH₄ and Pd-403-KBH₄ are 7.4 and 9.7 nm, respectively. HRTEM image (Fig. 6i) shows clear lattice fringes with a spacing of ca. 0.22 nm, which agrees well with the $d_{(111)}$ spacing of Pd.

The TEM images of Pd-373-H₂ and Pd-373-N₂H₄-H₂O are also shown in Fig. 6. As for the Pd-373-H₂ sample (Fig. 6j), besides the ordered double gyroid Pd networks, relatively large bulk Pd particles were also observed, which was probably due to the overflow of migrating Pd species to the external surface of the mesoporous silica template during the reduction process at a relatively high temperature (573 K). For Pd-373-N₂H₄-H₂O (Fig. 6k), some disordered networks rather than Pd particles were observed in addition to the ordered double gyroid Pd networks. Based on the TEM results, the regularity of the double gyroid Pd network catalysts decreases in the order of Pd-373-KBH₄ > Pd-373-N₂H₄-H₂O > Pd-373-H₂.

3.5. Morphology

HRSEM was further used to explore the morphology of the prepared mesoporous Pd catalysts. The HRSEM images in Fig. 7 show the typical mesoporosity of Pd catalysts replicated from KIT-6 templates prepared at different temperatures and reduced by different reducing agents. As shown in Fig. 7a and b, uncoupled gyroid networks with open pore system (I4₁32 symmetry) were clearly observed in Pd-308-KBH₄ and Pd-353-KBH₄ catalysts. In contrast, the Pd-373-KBH₄ and Pd-403-KBH₄ catalysts exhibited well-coupled and interpenetrated double gyroid networks with Ia3d symmetry (Fig. 7c and d). As for the Pd-373-N₂H₄-H₂O (Fig. 7e) and Pd-373-H₂ (Fig. 7f), some disordered networks or large Pd particles may be observed in addition to the ordered double gyroid networks, which are consistent with the above TEM observations.

Based on the HRSEM findings, the aforementioned N₂ physisorption, low-angle XRD and TEM results, it is indicated that our impregnation method is effective for creating free-standing Pd mesoporous networks. KIT-6 synthesized at high temperatures can be replicated with better quality. The topology of the replicated mesoporous Pd network catalysts can be tuned by changing the hydrothermal treatment temperature of the parent KIT-6 silica template. Specifically, when the hydrothermal treatment temperature of the KIT-6 is ≥ 373 K, double gyroid Pd networks with Ia3d symmetry can be created, while when the hydrothermal treatment temperature of the KIT-6 is ≤ 353 K, single gyroid mesoporous Pd

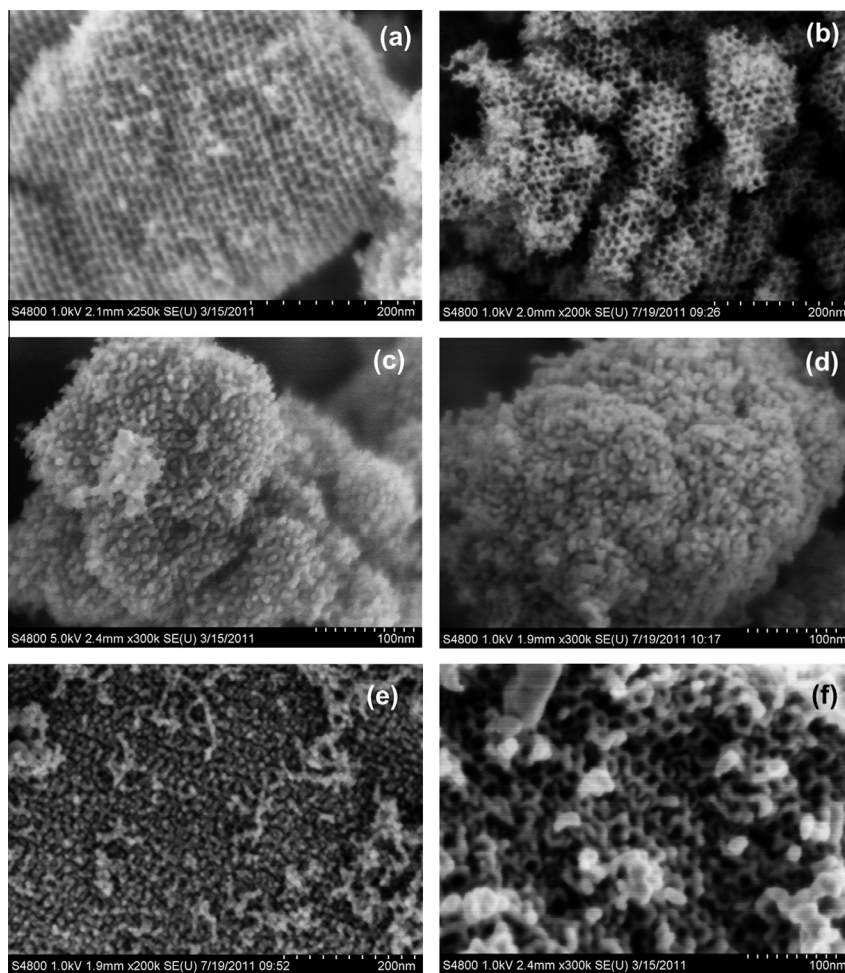


Fig. 7. HRSEM images of (a) Pd-308-KBH₄, (b) Pd-353-KBH₄, (c) Pd-373-KBH₄, (d) Pd-403-KBH₄, (e) Pd-373-N₂H₄-H₂O and (f) Pd-373-H₂ catalysts.

networks with $I4_132$ symmetry are formed. Among different reducing agents, the KBH_4 -reduced mesoporous Pd network catalyst exhibits more ordered gyroid structure than the $\text{N}_2\text{H}_4\cdot\text{H}_2\text{O}$ and H_2 -reduced samples.

3.6. Enantioselective hydrogenation of acetophenone

3.6.1. Influence of proline on C=O selectivity and enantioselectivity

The S-proline plays a specific role in the enantioselective hydrogenation of acetophenone. Without adding S-proline, the reactant was almost completely converted to ethylbenzene over the mesoporous Pd catalysts within 15 min and no enantioselectivity was observed. After adding S-proline in the reaction mixture, the mesoporous Pd catalyst exhibited a lower activity, but with much increased selectivity to 1-phenylethanol (C=O hydrogenation product). With increasing the molar ratio of S-proline/Pd, both the maximum yield of 1-phenylethanol and the enantioselectivity increased and reached a maximum at the molar ratio of 7.4:1. Then the enantioselectivity decreased dramatically with excessive amount of S-proline (Fig. S1). Thus, in our present study, the molar ratio of proline/Pd was kept to be 7.4:1 over all the mesoporous Pd catalysts.

Tungler et al. [6] proposed that the S-proline acted as a chiral auxiliary which reacted with acetophenone in solution to form a chiral condensation adduct with high diastereoselectivity. In their experiments, the methanolic solution of acetophenone and S-proline was boiled for 5 min to prepare the condensation product, which was evidenced by the disappearing of the C=O vibration band at 1685 cm^{-1} in acetophenone [32]. The hydrogenolysis of the resultant adduct on the Pd surface led to the formation of the chiral 1-phenylethanol. In such case, the ee is purely driven by the formation of the chiral adduct, and the higher S-proline concentration will improve ee without significant effects on the yield.

However, in our case, the hydrogenation reaction started immediately after the addition of acetophenone into the methanolic solution of S-proline with the gyroid Pd catalysts at 273 K. Therefore, the formation of S-proline-acetophenone adduct in solution is less likely, which is evidenced by the FTIR observation of C=O stretching mode in the reaction mixture (Fig. 8). Furthermore, our Gaussian calculations (B3LYP functional and 6-31G* basis set) [51] reveal that the formation of the condensation adduct between acetophenone and S-proline is an endothermic process and the Gibbs free energy difference between the condensation adduct and the acetophenone and S-proline at 273 K without considering the solvent effects is $+23.4\text{ kcal mol}^{-1}$. Thus, the condensation

adduct could not be formed under our present reaction conditions. To further ensure that the reaction is not driven by kinetic resolution through condensation between S-proline and acetophenone, we substituted S-proline with R-proline in the asymmetric hydrogenation of acetophenone and found that the (S)-1-phenylethanol instead of (R)-1-phenylethanol was formed in excess, verifying that the current reaction is indeed a Pd surface driven asymmetric reaction. The enantioselectivity achieved from our free-standing gyroid Pd catalysts in the present work is probably determined by the co-adsorbed S-proline and acetophenone on the metal surface. Due to the large surface area of the mesoporous Pd catalysts and the weak adsorption of S-proline on the Pd surface, a large amount of S-proline is needed in order to ensure enough adsorbed S-proline on the Pd surface for achieving high enantioselectivity. On the other hand, if the S-proline concentration is too high, the excessive S-proline probably also blocks the Pd active sites adjacent to the adsorbed S-proline, resulting in the decrease in both ee and yield.

3.6.2. Theoretical calculations

For better understanding the chiral recognition of S-proline on the Pd catalyst and to gain an insight into the reaction mechanism, the adsorptions of S-proline, acetophenone and their interaction conformations were calculated using the DFT methods. The adsorption energies for both the enantio-differentiating prochiral-R and prochiral-S intermediate complexes were quantitatively evaluated. Judging from the above HRTEM images (Fig. 6i) and the XRD analysis in Section 3.3, the crystalline plane preferred exposed in the mesoporous Pd network catalysts is the Pd(111) plane. Since it is not yet possible to mimic the Pd surface in the mesoporous gyroid structure in the theoretical calculations, we tentatively used flat Pd(111) surface with a (5×5) surface unit cell as a model plane for the calculation.

The adsorption geometry of the phenyl ring in acetophenone on Pd(111) is expected to be similar to that of benzene, dominated by the π -d interaction between the phenyl ring and the Pd(111). For benzene adsorbed on Pd(111), the bridge site was found to be the most stable adsorption site followed by the hollow site [52,53]. Our calculation results using the periodic slab are in accordance with the literature [52,53]. Thus, based on the above adsorption results of benzene, three reasonable adsorption modes of acetophenone were considered as the starting geometries for optimization in our calculations. In the first geometry, the adsorption is via the bonding of keto-carbonyl moiety to the Pd surface (denoted as the carbonyl adsorption mode), while the phenyl ring is on a hybrid between bridge and hollow sites. In the second geometry, the benzene moiety is adsorbed on a bridge site (denoted as bridge adsorption mode), which hinders the direct interaction of the carbonyl with the Pd surface atoms. The third one is similar to the second one except that the benzene moiety is adsorbed on a hollow site. Geometry optimization obtains only two stable adsorption configurations (Fig. 9). One is the carbonyl adsorption mode and the other is the bridge adsorption mode with corresponding adsorption energies of -22.8 and $-21.2\text{ kcal mol}^{-1}$, respectively. Thus, the carbonyl adsorption structure is slightly more stable than the bridge adsorption mode. The C=O bond in the carbonyl adsorption mode is elongated marginally (1.30 \AA) as compared to that in the bridge adsorption mode (1.26 \AA).

The geometry and adsorption energy of the isolated S-proline molecule adsorbed on the Pd(111) surface were also calculated with three most likely adsorption structures. As an amino acid molecule, both the pyrrolidine ring and the carboxylic group are possible to bond directly on Pd. So, the first starting geometry is the adsorption through the N atom in the pyrrolidine ring (denoted as N-adsorption mode). The second one is the adsorption through the hydrogen atoms in the pyrrolidine ring (denoted as

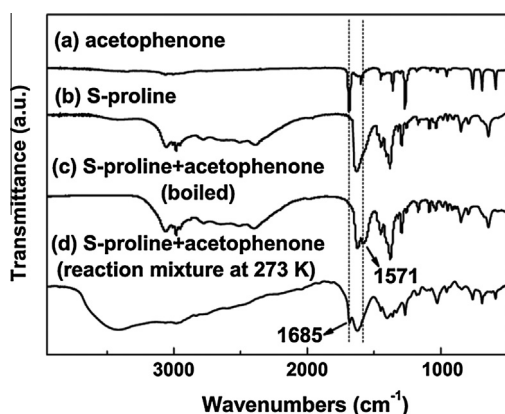


Fig. 8. FTIR spectra of (a) the methanolic solution of acetophenone, (b) the methanolic solution of S-proline, (c) the methanolic mixture of S-proline and acetophenone boiled at 363 K for 5 min, and (d) the reaction mixture of S-proline and acetophenone mixed at 273 K.

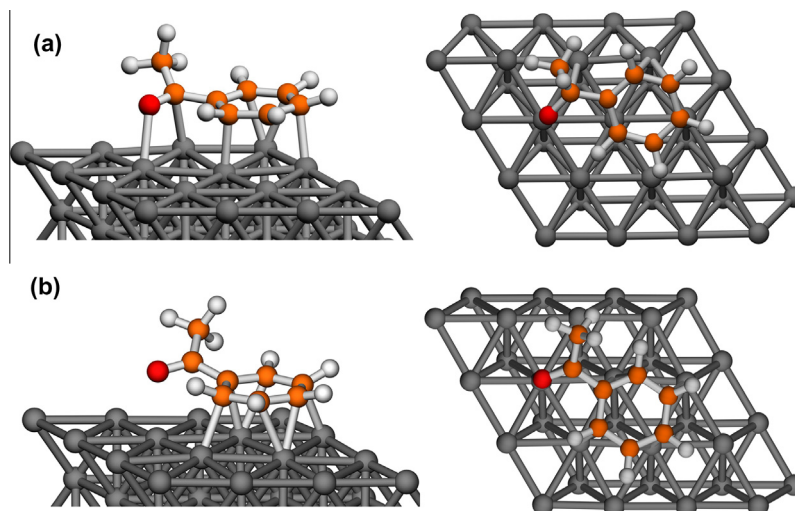


Fig. 9. Adsorption of acetophenone on the Pd slab. (a) Adsorption through the carbonyl; (b) Adsorption through benzene moiety (bridge).

H-adsorption mode). The third one is the adsorption through the oxygen atoms in the carboxylate group (denoted as O-adsorption mode). Since S-proline was adsorbed on Pd(111) as a zwitterion based on XPS study [54], the N atom is saturated and the N-adsorption mode is not possible. We, therefore, only optimized the H- and O-adsorption modes and the optimized geometries are shown in Fig. 10. The adsorption energies for the H- and O-adsorption mode are -10.4 and -14.1 kcal mol $^{-1}$, respectively, indicating that the adsorption through the carboxylic group in the form of a zwitterion is the most favorable structure. Meanwhile, in the optimized H-adsorption mode, S-proline is not present as a zwitterion, which is inconsistent with the experimental results [54]. Therefore, we only focused on the O-adsorption mode with the oxygen atoms of the carboxylate group close to the Pd surface and the pyrrolidine ring tilting above the carboxylate group in the following studies.

Taking the optimized adsorption geometries of acetophenone and S-proline, the interaction conformations between the co-adsorbed S-proline and acetophenone on Pd(111) surface were also calculated in order to identify the influence of S-proline on the adsorption of acetophenone. The optimized prochiral-R and prochiral-S geometries are shown in Fig. 11. It should be noted that by using acetophenone either in the carbonyl or bridge adsorption mode as the starting geometry, the resultant optimized interaction conformation is identical, which corresponds to the distorted bridge adsorption of acetophenone associated with the O-adsorption of S-proline as shown in Fig. 11. More importantly, we also

found that the existence of a hydrogen bonding between the oxygen atom of the carbonyl group in acetophenone and the hydrogen atom of the amino group in S-proline, which could play a significant role in the molecular chiral recognition. This hydrogen bonding interaction forces the carbonyl group in acetophenone to be away from the Pd surface. Meanwhile, this hydrogen bonding interaction forces the S-proline molecule to be closer to the Pd surface, resulting in the stronger interaction between S-proline and the Pd surface. Such subtle adjusting of the adsorption geometry of the acetophenone would be responsible for avoiding complete hydrogenation to form ethylbenzene and more importantly, resulting in high enantioselectivity.

The adsorption energies of the prochiral-R and prochiral-S interaction complex are -52.8 and -48.7 kcal mol $^{-1}$, respectively, which are more negative than the sum of the adsorption energies of the separately adsorbed acetophenone and S-proline. The calculated distances between the carbonyl oxygen and the hydrogen of the amino group in prochiral-R and prochiral-S complexes are 1.52 and 1.82 Å, respectively. These data suggest that there is an interaction between the co-adsorbed acetophenone and S-proline on the Pd surface. The energy difference between the prochiral-R and prochiral-S complexes is -4.1 kcal mol $^{-1}$, indicating that the prochiral-R complex is more stable and favors a higher fraction coverage on Pd surface. Thus, after subsequent hydrogen additions, (R)-1-phenylethanol is formed preferentially, which is in good accordance with the experimental results.

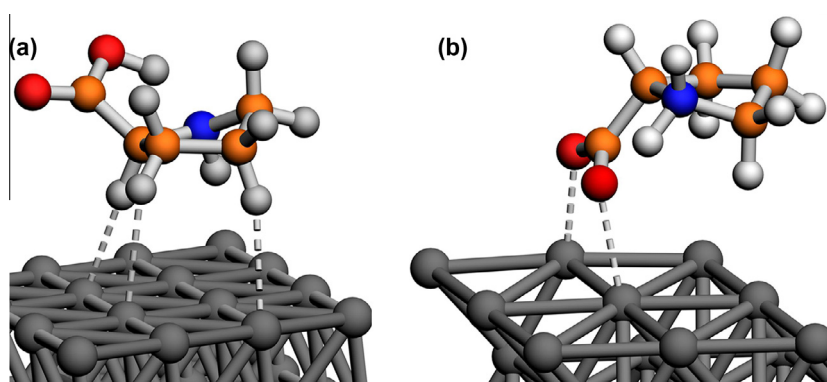


Fig. 10. Adsorption of S-proline on the Pd slab. (a) Adsorption through the hydrogen atoms in the pyrrolidine ring; (b) Adsorption through the oxygen atoms in the carboxylate group.

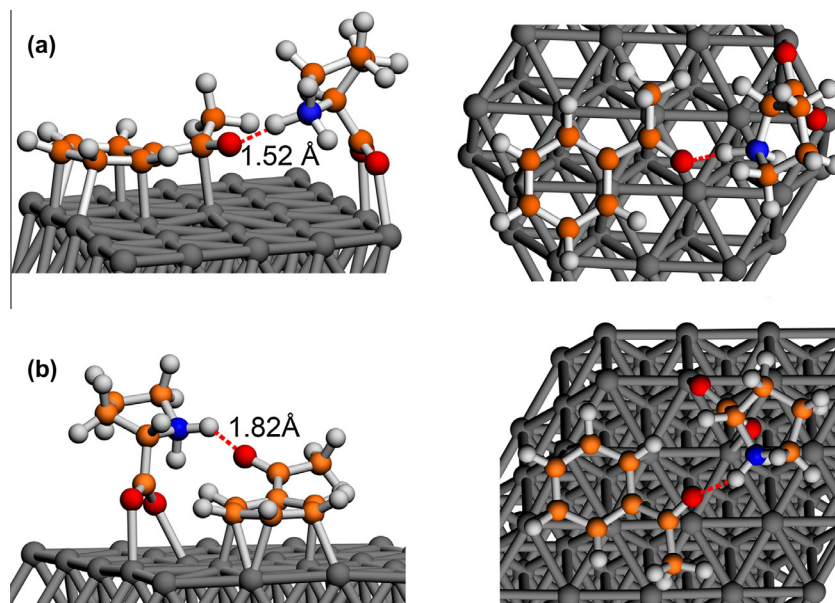


Fig. 11. The interaction conformation of S-proline with acetophenone. (a) Prochiral-R interaction conformation, leading to (R)-1-phenylethanol upon hydrogenation; (b) Prochiral-S interaction conformation, leading to (S)-1-phenylethanol upon hydrogenation.

3.6.3. Effect of Pd lattice structure on enantioselectivity

The effect of lattice structures on the catalytic performance was investigated by using the mesoporous Pd catalysts replicated from the same KIT-373 template but prepared by different reduction methods. The catalytic results for liquid phase enantioselective hydrogenation of acetophenone with a fixed reaction time of 15 min are compiled in Table 3. When H₂ was used as the reducing agents for creating Pd networks, the fastest hydrogenation rate was achieved with the 1-phenylethanol yield of 48.9% and the ee of ca. 22%. When N₂H₄·H₂O was used as the reducing agent, the yield of 1-phenylethanol is reduced to 24.2% while the ee is increased to 30%. When KBH₄ was used as the reducing agent, the ee is further increased to 34% with the yield of 1-phenylethanol reduced to 12.8%. Therefore, the enantioselectivities are in the sequence of Pd-373-KBH₄ > Pd-373-N₂H₄·H₂O > Pd-373-H₂ catalyst, while the 1-phenylethanol yields are in the reverse order. As discussed above in Section 3.3, the Pd-373-KBH₄ catalyst has the highest preferred orientation of the (111) plane among the three catalysts. Thus, the Pd-373-KBH₄ catalyst has higher density of flat surfaces with less surface kinks and steps, which is possibly more appropriate to accommodate the bulky prochiral complex that occupies minimum 13 surface atoms, resulting in the highest enantioselectivity. Also, the above TEM and HRSEM results revealed that in addition to

Table 3
Catalytic behaviors of mesoporous Pd catalysts in the enantioselective hydrogenation of acetophenone.^a

Catalyst	Topology ^b	1-Phenylethanol yield (%)	ee (%)
Pd-308-KBH ₄	I4 ₁ 32	12.6	31 (R)
Pd-353-KBH ₄	I4 ₁ 32	19.1	31 (R)
Pd-373-KBH ₄	Ia3d	12.8	34 (R)
Pd-403-KBH ₄	Ia3d	13.3	42 (R)
Pd-373-N ₂ H ₄ ·H ₂ O	Ia3d	24.2	30 (R)
Pd-373-H ₂	Ia3d	48.9	22 (R)
Hexagonal Pd nanoarray	P6mm	48.7	28 (R)
Ultrafine Pd black	–	82.0	20 (R)

^a Reaction conditions: 0.02 mL acetophenone, 0.40 g S-proline, 17 mL of methanol, T = 273 K, H₂ flow rate of 60 mL min⁻¹, W_{cat} = 0.050 g, reaction time = 15 min.

^b Topology derived based on the low-angle XRD, N₂-physisorption, TEM and HRSEM results.

the ordered double gyroid networks, there are some disordered networks or bulk Pd nanoparticles existed in the Pd-373-N₂H₄·H₂O and Pd-373-H₂ catalysts. The high quality gyroid structure in Pd-373-KBH₄ catalyst may also contribute to its superior enantioselectivity as compared to the Pd-373-N₂H₄·H₂O and Pd-373-H₂ catalysts.

3.6.4. Effect of template topology on enantioselectivity

The effect of the topology on the catalytic performance was investigated by using the KBH₄-reduced mesoporous Pd catalysts replicated from the silica template synthesized at different temperatures. The catalytic results of the mesoporous Pd catalysts with different topologies (space group I4₁32 and Ia3d) are also compiled in Table 3. For comparison, the catalytic results of ultrafine Pd black and hexagonal Pd nanoarray catalyst with the space group of P6mm are also shown. The ee over ultrafine Pd black is ca. 20% with the yield of 1-phenylethanol of ca. 82.0% after a reaction of 15 min. In comparison, the ee over hexagonal Pd nanoarray catalyst is 28%, which is much higher than that over ultrafine Pd black. The ee is further increased to 31–42% over the Pd-x-KBH₄ catalysts with single or double gyroid structure. Generally, the enantioselectivity over the mesoporous Pd catalysts is in the sequence of double gyroid structure (Ia3d) > single gyroid structure (I4₁32) > hexagonal structure (P6mm) > ultrafine Pd black. Since the gyroid Pd-x-KBH₄ catalysts and hexagonal Pd nanoarray catalyst were prepared under the same reduction condition but using silica templates with different topology, it is plausible to attribute the variation of enantioselectivity to the different topology of the original silica template. The unique spatial arrangement of the Pd crystallites in the gyroid structure enhances the interaction conformation of the co-adsorbed acetophenone and the chiral S-proline modifier to form the R-isomer of 1-phenylethanol preferentially. In contrast, the ultrafine Pd black catalyst without such steric constraint exhibited the lowest enantioselectivity.

3.6.5. Effect of pore size on enantioselectivity

The effect of pore size on the catalytic performance was further investigated by using KBH₄-reduced mesoporous gyroid Pd catalysts with the same topology but different pore diameter (Table 3). As for the single gyroid structures (Pd-308-KBH₄ and Pd-353-

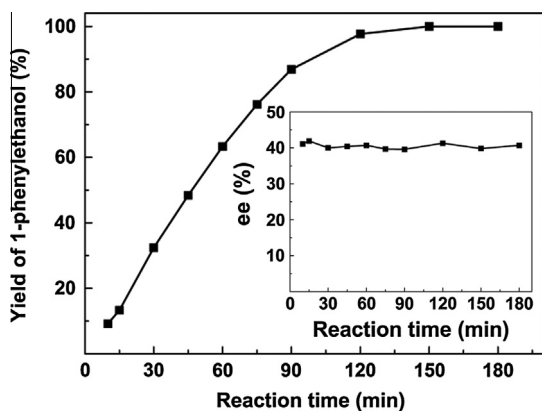


Fig. 12. The yield of 1-phenylethanol and the evolution of the enantioselectivity (inset) as a function of the reaction time over the Pd-403-KBH₄ catalyst. Reaction conditions: 0.02 mL of acetophenone, 0.40 g S-proline, 17 mL of methanol, $T = 273$ K, H_2 flow rate of 60 mL min^{-1} , $W_{\text{cat.}} = 0.050$ g.

KBH₄), they have only large pores and the change of the pore size seems to have little effect on the enantioselectivity. Nearly the same ee values were obtained over the Pd-308-KBH₄ and Pd-353-KBH₄ catalysts with different pore size of ca. 13.1 and 11.0 nm, respectively. As for the double gyroid structure, the enantioselectivity over Pd-403-KBH₄ is 42%, which is higher than that over Pd-373-KBH₄ (34%). As discussed in Section 3.1, Pd-373-KBH₄ and Pd-403-KBH₄ exhibit bimodal pore size distribution with the small pore at ca. 4.1 or 2.1 nm, respectively, along with the large pore at ca. 11–13 nm. The large pores in all the gyroid structures (single and double) are expected to contribute to a similar level of ee. Therefore, the additional enhancement of ee from the double gyroid Pd catalysts may result from the presence of small pores. Such enhancement can be attributed to the confinement effects related to the small pores which generate stronger steric constraints of the adsorbates and improve the intermolecular interaction between the co-adsorbed reactant and the chiral modifier.

3.6.6. Catalytic behavior of the optimized Pd-403-KBH₄ catalyst

In order to have a better insight into the catalytic performance of the optimized Pd-403-KBH₄ catalyst, the reaction course was

recorded (Fig. 12). The yield of 1-phenylethanol over the Pd-403-KBH₄ catalyst increased gradually to 100% at a reaction time of 150 min and remained constant at prolonged reaction time, clearly demonstrating its excellent selectivity to the C=O group. The enantioselectivity of the system is very stable with a value of 42%, which is much higher than that over the ultrafine Pd black catalyst (ca. 20%), signifying the superior enantioselective property of the Pd-403-KBH₄. The stability of the enantioselectivity over the Pd-403-KBH₄ catalyst was further verified in three successive runs. No reduction in yield and ee were observed and the mesostructure of the used catalyst is maintained, which can be attributed to the benefit of low reaction temperature and the superior structural strength of the highly interconnected double gyroid Pd networks.

3.7. Enantioselective hydrogenation of ring-substituted acetophenone derivatives

The catalytic performances of the Pd-403-KBH₄ catalyst in the enantioselective hydrogenation of ring-substituted acetophenone derivatives were also investigated. As shown in Table 4, the ee of the hydrogenation reaction decreases to below 16% when a H atom in the aromatic ring is replaced by an electron-donating $-\text{OCH}_3$ group. However, the ee increases to $\sim 73\%$ when $-\text{H}$ is replaced by an electron-withdrawing $-\text{CF}_3$ group. This suggests that the mesoporous Pd catalyst may be promising in the enantioselective hydrogenation of the acetophenone derivatives with electron-withdrawing groups. For $-\text{CF}_3$ substituted acetophenones, both the ee value and the yield were affected by the substitution positions. From para, meta to ortho position, the ee increases from 42% to 73%, while the yield decreases dramatically. The TOF values calculated on the basis of the active surface area of the Pd-403-KBH₄ catalyst as determined by CO chemisorption ($13.3 \text{ m}^2 \text{ g}_{\text{Pd}}^{-1}$) are also summarized in Table 4. In most cases, the R-enantiomer is dominant except that in the case of $\text{OCH}_3(\text{ortho})$ -substituted acetophenone.

For a better understanding of how the substituent groups affect the enantioselectivity and more importantly why the inversed chiral recognition is occurred in the case of $\text{OCH}_3(\text{ortho})$ -substituted acetophenone, the interaction conformations of the co-adsorbed substituted acetophenone and S-proline over the Pd(111) surface were calculated using the DFT methods. The adsorption energies

Table 4
Catalytic behaviors of Pd-403-KBH₄ catalyst in the enantioselective hydrogenation of acetophenone and ring-substituted acetophenones.^a

Reactant	Reaction time (min)	Yield (%)	TOF (S^{-1})	Maximum ee (%)	$E_{\text{ads.}}^{\text{b}}$ (kcal mol^{-1})		ΔE^{c} (kcal mol^{-1})
					Prochiral-R	Prochiral-S	
	15	13.3	1.8×10^{-3}	42 (R)	-52.8	-48.7	-4.1
	780	2.2	4.5×10^{-6}	73 (R)	-64.6	-56.7	-7.9
	15	6.5	6.9×10^{-4}	50 (R)	-68.0	-62.7	-5.3
	60	19.6	5.2×10^{-4}	42 (R)	-68.0	-65.0	-3.0
	480	3.7	1.3×10^{-5}	8 (S)	-69.9	-70.3	0.4
	240	12.2	8.8×10^{-5}	16 (R)	-73.3	-71.9	-1.4

^a Reaction conditions: 0.02 mL substrate, 0.40 g S-proline, 17 mL of methanol, $T = 273$ K, H_2 flow rate of 60 mL min^{-1} , $W_{\text{cat.}} = 0.050$ g.

^b Adsorption energies calculated using the SIESTA package with a double-polarization (DZP) basis set.

^c Energy difference between prochiral-R and prochiral-S intermediate complexes.

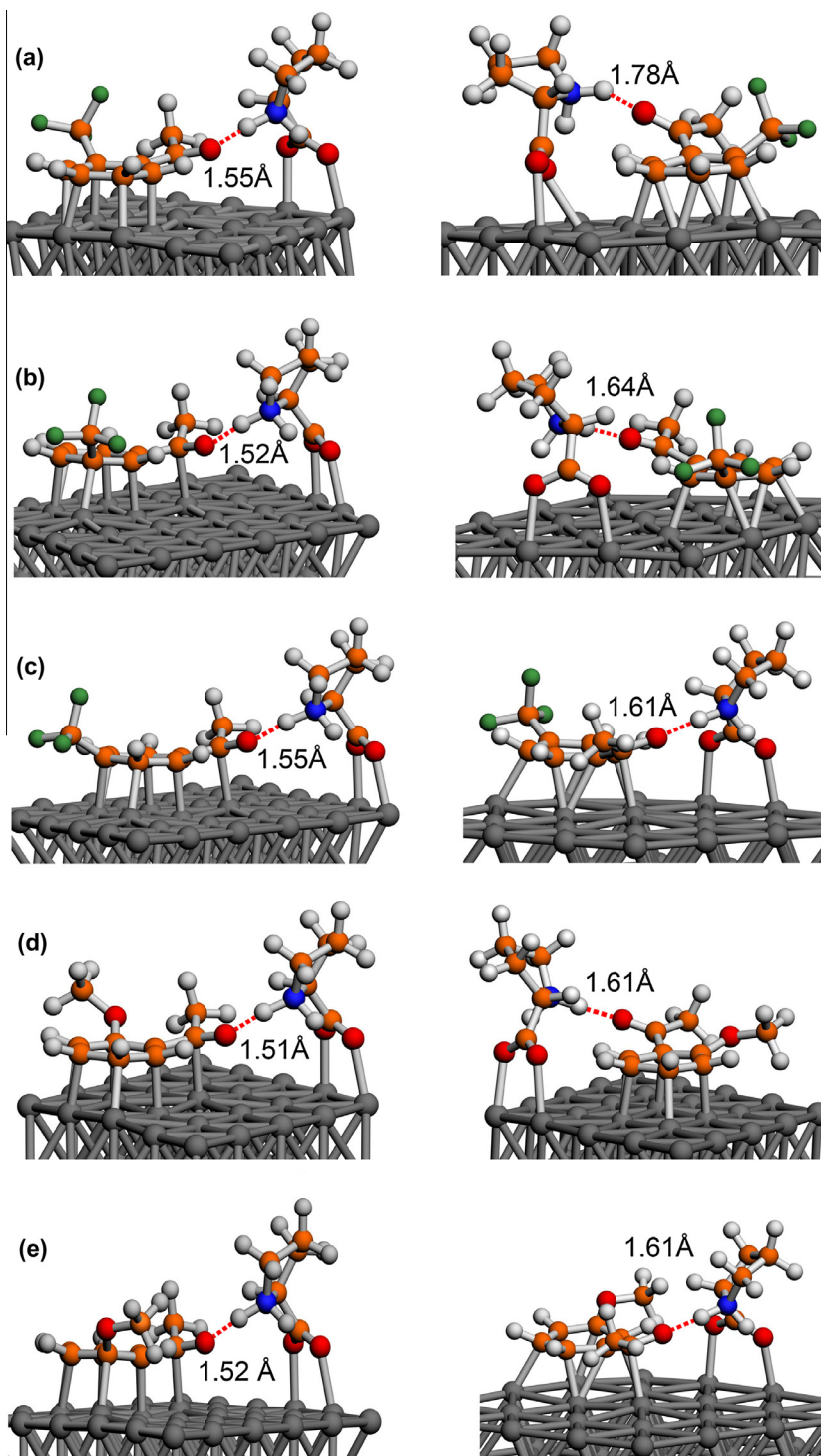


Fig. 13. The prochiral-R (left) and prochiral-S (right) interaction conformation of S-proline with substituted acetophenone. (a) CF_3 (ortho)-substituted acetophenone; (b) CF_3 (meta)-substituted acetophenone; (c) CF_3 (para)-substituted acetophenone; (d) OCH_3 (ortho)-substituted acetophenone; (e) OCH_3 (meta)-substituted acetophenone.

of the prochiral-R and prochiral-S interaction complexes and their energy differences are shown in Table 4 and the optimized interaction conformations are shown in Fig. 13. It was found that after ring-substitution by either $-\text{CF}_3$ or $-\text{OCH}_3$, the interaction between the substituted acetophenones, S-proline and the Pd surface was improved. In most cases, the adsorption energies for the prochiral-R complexes are more negative than those for the prochiral-S complexes, resulting in the dominant R-enantiomer. In contrast,

for OCH_3 (ortho)-substituted acetophenone, the adsorption energy of the prochiral-S complex is slightly more negative than that of the prochiral-R complex. Thus, after subsequent hydrogen additions, the S-enantiomer is formed in excess, which is in good accordance with the experimental results.

Further inspection of our experimental results and our DFT calculations leads us to conclude that the enantio-differentiation in the enantioselective hydrogenation of acetophenone derivatives

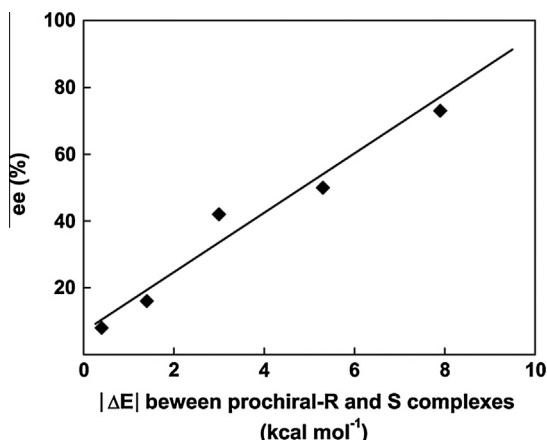


Fig. 14. The enantioselectivity in the hydrogenation of ring-substituted acetophenones over the Pd-403-KBH₄ catalyst as a function of the absolute value of the calculated adsorption energy difference between the prochiral-R and prochiral-S intermediate complexes.

over S-proline modified Pd catalysts could be correlated with the relative adsorption energies of the optimized prochiral-R and prochiral-S intermediate complexes. To demonstrate such a correlation, a plot of ee versus the absolute value of the adsorption energy difference between the prochiral-R and prochiral-S intermediate complexes is shown in Fig. 14, which gives a good linear relationship. The larger the absolute value of the adsorption energy difference (ΔE) between the prochiral-R and prochiral-S intermediate complexes, the higher the ee obtained. Such correlation confirms that the achieved ee is determined by the chiral specific interactions. It is worth noting that the ΔE between the prochiral-R and prochiral-S intermediate complexes we obtained in our present theoretical calculations is not exactly equal to the difference in the Gibbs free energy (ΔG) in the catalytic system. Due to the size of the theoretical model used and the limits of the current computing power, it is still infeasible to calculate the ΔG in our present catalytic system. One would expect that, at 273 K, a ΔG of ca. 3 kcal mol⁻¹ results in a predicted ee of ~100%. However, as shown in Fig. 14, much lower ee (~42%) was obtained in our experiment compared to the predicted values (~100% ee) with the ΔE of ca. 3 kcal mol⁻¹. The observed difference between ΔE and ΔG is probably related to the limitation of the present theoretical calculation model, which is impossible to completely mimic the real catalytic surface. The energetically favored complex leads to the formation of the corresponding enantiomer in excess upon hydrogenation. Similar theoretical calculations have earlier been made for the Pt-cinchona system in the hydrogenations of ketopantolactone [55] and methyl pyruvate [56,57] by Baiker and coworkers. In those studies a good agreement between the stability of the prochiral-R and prochiral-S complexes and the stereochemical outcome of the reactions were also found, where purely thermodynamic considerations were used for predicting the major enantiomer. It is interesting that this approach apparently also works for our Pd-proline system to predict the major enantiomeric product.

4. Conclusions

The factors influencing the confinement effect originated from the nanopores such as the topology, pore size, and lattice structure of the free-standing mesoporous Pd network catalysts and their correlation with the catalytic performances in the enantioselective hydrogenation of acetophenone and its derivatives were studied. It was found that the confinement effect was very important in determining the enantioselectivity of the reaction. By manipulating

the topology, pore size and lattice structure of the mesoporous Pd network catalysts, the enantioselectivity of the reaction could be tuned. The enantioselectivity over the mesoporous Pd catalysts increases in the sequence of double gyroid structure (Ia3d) > single gyroid structure (I4₁32) > 2D hexagonal structure (P6mm) > ultra-fine Pd black. The relatively smaller pore diameter within the double gyroid structures is favorable to achieve higher ee. Among H₂, N₂H₄·H₂O and KBH₄, KBH₄ was found to be the best reducing agents to obtain high quality replicated gyroid Pd networks with proper lattice structure, which is important to achieve high enantioselectivity. The unique spatial arrangement of Pd crystallites in the double gyroid structure with a proper pore size and the desired lattice structure formed by KBH₄ reduction provided suitable microenvironment to generate optimized confinement effect, which improved the enantio-differentiation. The optimized Pd-403-KBH₄ catalyst exhibits relatively high ee of ~42% in the enantioselective hydrogenation of acetophenone and ee up to 73% in the -CF₃ substituted acetophenone derivatives. DFT studies reveal that the major enantiomeric product could be predicted by the relative energy difference between the optimized prochiral-R and prochiral-S intermediate complexes formed by the acetophenone and its derivatives with S-proline. The energetically favored intermediate complex leads to the formation of the corresponding enantiomer in excess upon hydrogenation. The ee was linearly correlated with the adsorption energy difference between prochiral-R and prochiral-S complexes. Our work presents a new possibility for tuning the enantioselectivity by manipulating the confinement effect in the free-standing mesoporous Pd catalysts and provides useful information for understanding the chiral recognition mechanism, which is also helpful to provide guidance for the design of highly efficient enantioselective metal catalysts in heterogeneous asymmetric hydrogenation.

Acknowledgments

This work was supported by the National Natural Science Foundation of China (21343003, 20803009), the Shanghai Science and Technology Committee (12ZR1401400) and the Ministry of Education (the Scientific Research Foundation for the Returned Overseas Chinese Scholars).

Appendix A. Supplementary material

Supplementary data associated with this article can be found, in the online version, at <http://dx.doi.org/10.1016/j.jcat.2014.03.004>.

References

- [1] E.N. Jacobsen, A. Pfaltz, H. Yamamoto, *Comprehensive Asymmetric Catalysis*, Springer, Berlin, 1999.
- [2] E. Klabunovskii, G.V. Smith, Á. Zsigmond, *Heterogeneous Enantioselective Hydrogenations – Theory and Practice*, Springer, Dordrecht, 2006.
- [3] R.A. Sheldon, *Pure Appl. Chem.* 72 (2000) 1233.
- [4] G.V. Smith, F. Notheisz, *Heterogeneous Catalysis in Organic Chemistry*, Academic Press, San Diego, 1999.
- [5] H.U. Blaser, B. Pugin, *Chiral Reactions in Heterogeneous Catalysis*, Plenum Press, New York, 1995.
- [6] A. Tüngler, T. Tarnai, T. Mathe, J. Petro, *J. Mol. Catal.* 67 (1991) 277.
- [7] A. Perosa, P. Tundo, M. Selva, *J. Mol. Catal. A – Chem.* 180 (2002) 169.
- [8] R. Hess, T. Mallat, A. Baiker, *J. Catal.* 218 (2003) 453.
- [9] R. Hess, A. Vargas, T. Mallat, T. Burgi, A. Baiker, *J. Catal.* 222 (2004) 117.
- [10] R. Hess, F. Krumeich, T. Mallat, A. Baiker, *J. Mol. Catal. A – Chem.* 212 (2004) 205.
- [11] V. Vetere, M.B. Faraoni, G.F. Santori, J.C. Podesta, M.L. Casella, O.A. Ferretti, *J. Catal.* 226 (2004) 457.
- [12] S. Basu, M. Mapa, C.S. Gopinath, M. Doble, S. Bhaduri, G.K. Lahiri, *J. Catal.* 239 (2006) 154.
- [13] T. Marzalletti, M. Oportus, D. Ruiz, J.L.G. Fierro, P. Reyes, *Catal. Today* 133 (2008) 711.
- [14] H. Cheng, J. Hao, H. Wang, C. Xi, X. Meng, S. Cai, F. Zhao, *J. Mol. Catal. A – Chem.* 278 (2007) 6.

- [15] B. Tang, W. Xiong, E.R. Liu, Y. Jia, J.B. Wang, H. Chen, X.J. Li, *Tetrahedron-Asymmetry* 19 (2008) 1397.
- [16] H.Y. Jiang, H. Chen, R.X. Li, *Catal. Commun.* 11 (2010) 584.
- [17] H.Y. Jiang, C.F. Yang, C. Li, H.Y. Fu, H. Chen, R.X. Li, X.J. Li, *Angew. Chem. Int. Ed.* 47 (2008) 9240.
- [18] C.F. Yang, H.Y. Jiang, J. Feng, H.Y. Fu, R.X. Li, H. Chen, X.J. Li, *J. Mol. Catal. A – Chem.* 300 (2009) 98.
- [19] C. Li, L. Zhang, Y. Du, X.L. Zheng, H.Y. Fu, H. Chen, R.X. Li, *Catal. Commun.* 28 (2012) 5.
- [20] M.M. Liu, B.B. Fan, X.F. Shi, R.F. Li, *Catal. Commun.* 42 (2013) 20.
- [21] C. Li, *Catal. Rev. – Sci. Eng.* 46 (2004) 419.
- [22] F. Hoxha, B. Schimmoeller, Z. Cakl, A. Urakawa, T. Mallat, S.E. Pratsinis, A. Baiker, *J. Catal.* 271 (2010) 115.
- [23] F. Hoxha, E. Schmidt, T. Mallat, B. Schimmoeller, S.E. Pratsinis, A. Baiker, *J. Catal.* 278 (2011) 94.
- [24] S.C. Warren, L.C. Messina, L.S. Slaughter, M. Kamperman, Q. Zhou, S.M. Gruner, F.J. DiSalvo, U. Wiesner, *Science* 320 (2008) 1748.
- [25] S.C. Warren, U. Wiesner, *Pure Appl. Chem.* 81 (2009) 73.
- [26] Y. Kuroda, Y. Yamauchi, K. Kuroda, *Chem. Commun.* 46 (2010) 1827.
- [27] Y. Yamauchi, K. Kuroda, *Chem. – Asian J.* 3 (2008) 664.
- [28] Y. Yamauchi, A. Takai, M. Komatsu, M. Sawada, T. Ohsuna, K. Kuroda, *Chem. Mater.* 20 (2008) 1004.
- [29] A. Takai, Y. Yamauchi, K. Kuroda, *J. Am. Chem. Soc.* 132 (2010) 208.
- [30] Y. Doi, A. Takai, Y. Sakamoto, O. Terasaki, Y. Yamauchi, K. Kuroda, *Chem. Commun.* 46 (2010) 6365.
- [31] A. Takai, Y. Doi, Y. Yamauchi, K. Kuroda, *J. Phys. Chem. C* 114 (2010) 7586.
- [32] X.Y. Chen, Z.Y. Lou, M.H. Qiao, K.N. Fan, S.C. Tsang, H.Y. He, *J. Phys. Chem. C* 112 (2008) 1316.
- [33] T.W. Kim, F. Kleitz, B. Paul, R. Ryoo, *J. Am. Chem. Soc.* 127 (2005) 7601.
- [34] V. Holler, K. Radevik, I. Yuranov, L. Kiwi-Minsker, A. Renken, *Appl. Catal. B – Environ.* 32 (2001) 143.
- [35] B.E. Warren, *J. Appl. Phys.* 12 (1941) 375.
- [36] L.A. Solovoyov, V.I. Zaikovskii, A.N. Shmakov, O.V. Belousov, R. Ryoo, *J. Phys. Chem. B* 106 (2002) 12198.
- [37] J. Junquera, O. Paz, D. Sanchez-Portal, E. Artacho, *Phys. Rev. B* 64 (2001).
- [38] N. Troullier, J.L. Martins, *Phys. Rev. B* 43 (1991) 1993.
- [39] J.P. Perdew, K. Burke, M. Ernzerhof, *Phys. Rev. Lett.* 77 (1996) 3865.
- [40] http://www.netlib.org/scalapack/scalapack_home.html.
- [41] A. Eichler, F. Mittendorfer, J. Hafner, *Phys. Rev. B* 62 (2000) 4744.
- [42] A. Rumpelcker, F. Kleitz, E.L. Salabas, F. Schuth, *Chem. Mater.* 19 (2007) 485.
- [43] J.K. Shon, S.S. Kong, J.M. Kim, C.H. Ko, M. Jin, Y.Y. Lee, S.H. Hwang, J.A. Yoon, J.N. Kim, *Chem. Commun.* (2009) 650.
- [44] F. Jiao, A.H. Hill, A. Harrison, A. Berko, A.V. Chadwick, P.G. Bruce, *J. Am. Chem. Soc.* 130 (2008) 5262.
- [45] Y.F. Shi, B.K. Guo, S.A. Corr, Q.H. Shi, Y.S. Hu, K.R. Heier, L.Q. Chen, R. Seshadri, G.D. Stucky, *Nano Lett.* 9 (2009) 4215.
- [46] O. Bisi, O. Jepsen, O.K. Andersen, *Phys. Rev. B* 36 (1987) 9439.
- [47] B.Z. Tian, X.Y. Liu, L.A. Solovoyov, Z. Liu, H.F. Yang, Z.D. Zhang, S.H. Xie, F.Q. Zhang, B. Tu, C.Z. Yu, O. Terasaki, D.Y. Zhao, *J. Am. Chem. Soc.* 126 (2004) 865.
- [48] H.J. Shin, R. Ryoo, Z. Liu, O. Terasaki, *J. Am. Chem. Soc.* 123 (2001) 1246.
- [49] C.S. Barrett, T.B. Massalski, *Structure of Metals*, Pergamon Press, Oxford, 1980.
- [50] V. Saranathan, C.O. Osuji, S.G.J. Mochrie, H. Noh, S. Narayanan, A. Sandy, E.R. Dufresne, R.O. Prum, *Proc. Natl. Acad. Sci.* 107 (2010) 11676.
- [51] M.J. Frisch, G.W. Trucks, H.B. Schlegel, G.E. Scuseria, M.A. Robb, J.R. Cheeseman, J.A. Montgomery, Jr., T. Vreven, K.N. Kudin, J.C. Burant, J.M. Millam, S.S. Iyengar, J. Tomasi, V. Barone, B. Mennucci, M. Cossi, G. Scalmani, N. Rega, G.A. Petersson, H. Nakatsuji, M. Hada, M. Ehara, K. Toyota, R. Fukuda, J. Hasegawa, M. Ishida, T. Nakajima, Y. Honda, O. Kitao, H. Nakai, M. Klene, X. Li, J.E. Knox, H.P. Hratchian, J.B. Cross, C. Adamo, J. Jaramillo, R. Gomperts, R.E. Stratmann, O. Yazyev, A.J. Austin, R. Cammi, C. Pomelli, J.W. Ochterski, P.Y. Ayala, K. Morokuma, G.A. Voth, P. Salvador, J.J. Dannenberg, V.G. Zakrzewski, S. Dapprich, A.D. Daniels, M.C. Strain, O. Farkas, D.K. Malick, A.D. Rabuck, K. Raghavachari, J.B. Foresman, J.V. Ortiz, Q. Cui, A.G. Baboul, S. Clifford, J. Cioslowski, B.B. Stefanov, G. Liu, A. Liashenko, P. Piskorz, I. Komaromi, R.L. Martin, D.J. Fox, T. Keith, M.A. Al-Laham, C.Y. Peng, A. Nanayakkara, M. Challacombe, P.M.W. Gill, B. Johnson, W. Chen, M.W. Wong, C. Gonzalez, J.A. Pople, *Gaussian 03, Revision B.04*, Gaussian Inc., Pittsburgh, PA, 2003.
- [52] F. Mittendorfer, C. Thomazeau, P. Raybaud, H. Toulhoat, *J. Phys. Chem. B* 107 (2003) 12287.
- [53] C. Morin, D. Simon, P. Sautet, *J. Phys. Chem. B* 108 (2004) 5653.
- [54] F. Gao, Y.L. Wang, L. Burkholder, W.T. Tysoe, *Surf. Sci.* 601 (2007) 3579.
- [55] M. Schurch, O. Schwalm, T. Mallat, J. Weber, A. Baiker, *J. Catal.* 169 (1997) 275.
- [56] T. Burgi, A. Baiker, *J. Catal.* 194 (2000) 445.
- [57] A. Baiker, *J. Mol. Catal. A – Chem.* 163 (2000) 205.